Vertical velocity of a small sphere in a sheared granular bed

Song Gao (高颂),[1] Julio M. Ottino,[1,2,3] Richard M. Lueptow,[1,2,3] and Paul B. Umbanhowar[1,*]

[1] *Department of Mechanical Engineering*
[2] *Department of Chemical and Biological Engineering*
[3] *Northwestern Institute on Complex Systems (NICO), Northwestern University, Evanston, Illinois 60208, USA*

(Dated: April 1, 2025)

Small particles fall through sheared beds of larger particles in settings ranging from geophysics to industry, but study of large-to-small size ratios, R, spanning the trapping threshold, R_t, has been neglected. In simulations of non-cohesive spheres for $R < R_t$, the small-sphere vertical velocity, v_p, first increases with shear rate, $\dot{\gamma}$, as trapping time decreases, but v_p then decreases as velocity fluctuations frustrate downward mobility. For $R > R_t$, v_p is constant at low $\dot{\gamma}$, but again decreases at high $\dot{\gamma}$. We model these behaviors and discuss analogies with electron transport in solids.

The movement of solid particles through porous media, i.e., *percolation*, is relevant in many scientific and engineering contexts. In granular materials, smaller particles fall through void spaces between larger particles. In geophysics, percolation of solids, like that for soil erosion or sediment transport in rivers, influences environmental sustainability, landscape dynamics, and ecological habitats. In biological systems, percolation occurs as the movement of nutrients through biological tissues and organs. In industry, percolation occurs in filtration systems for separation and packed beds for absorption. The percolation dynamics in these processes depend strongly on the relative particle size and pore structure (static and dynamic) of the porous media.

In mixtures of size-disperse granular materials, small-particle percolation leads to de-mixing (segregation), which is a critical issue in various natural [1–3] and industrial processes [4, 5]. Recent studies have advanced models of granular segregation (see, e.g., [6, 7]), but nearly all consider mixtures with large-to-small particle diameter ratios, $R \lesssim 2$, where interparticle contacts are enduring [8–10]. In these cases, segregation can be characterized by a concentration-dependent mean vertical velocity (i.e., the *percolation* velocity [11]), v_p, which increases monotonically with both R and shear rate, $\dot{\gamma}$.

For larger R, where the small particles are referred to as *fine* particles or *fines*, the v_p-dependence on $\dot{\gamma}$ and R in sheared flows changes significantly. In particular, for $R \gtrsim 2$ and low fines concentration, v_p increases dramatically with increasing R [11, 12], while, in contrast, v_p is nearly R-independent at larger fines concentration (above 10%) for $2 \lesssim R \lesssim 4$ [13]. Here we focus on fine-particle percolation in uniform shear flow in the zero-concentration limit, where an increasing tendency toward *free-sifting* or *spontaneous interparticle percolation* [14–17] (i.e., the downward motion of fines at $\dot{\gamma} = 0$) with increasing R leads to qualitative changes in the dependence of v_p on $\dot{\gamma}$ and other parameters. To focus on the effects of $\dot{\gamma}$ and R, we consider non-cohesive particle interactions, noting that cohesive forces profoundly affect the statics and dynamics of granular material when they are large relative to particle weight.

Free-sifting has been studied primarily in static beds for $R > R_t$ [16, 18–21], where the free-sifting threshold, R_t, is $R_{t0} = (2/\sqrt{3} - 1)^{-1} \approx 6.46$ for rigid monodisperse bed-spheres [22], but is larger in polydisperse mixtures of "soft" particles [23]. Free-sifting can also occur for $R < R_t$ in randomly packed static beds when a subset of pore throats—the minimum opening between neighboring bed spheres—exceeds the fine-particle diameter. In this case, motion is *transient* since a fine particle inevitably encounters an impassible pore throat [24] and is trapped. Despite the ubiquity of fines in industrial solids processing [25, 26], their potential for affecting the mobility of various geophysical flows [27–29], and their importance in sediment infiltration that shapes rivers [30, 31], few studies address the movement, or percolation, of fines through sheared granular beds [11, 12, 32].

In this paper we show that free-sifting is pronounced and unavoidably coupled with shear for $R < R_t$, because fines that would be trapped in a static bed are repeatedly re-mobilized by shear-induced particle rearrangements. In past work, the complexity of this problem and the limited parameter-space explored produced puzzling inconsistencies regarding the dependence of v_p on $\dot{\gamma}$ [32] and R [11–13]. Here we resolve these issues by characterizing the small-sphere vertical velocity in a larger-sphere bed for size ratios spanning the free-sifting threshold ($2 \leq R \leq 10$) and spatially-uniform shear rates covering the quasi-static and rapid dense flow regimes [33]. Our results reveal a non-monotonic dependence of v_p on $\dot{\gamma}$, provide relations for predicting v_p in the low- and high-shear-rate regimes, and add insight into the dominant physics in each regime. We also address similarities between gravitational-field driven fine-particle transport and electric-field driven conduction of electrons, where R_t delineates the boundary between semiconductor-like ($R < R_t$) and metal-like ($R > R_t$) transport regimes and $\dot{\gamma}$ acts similarly to temperature.

Methods—LIGGGHTS [34], a discrete element method code, is used to simulate single spheres of diameter d_f in a confined dense flow of bed particles of diameter,

d, with a prescribed horizontal velocity varying linearly with depth [35] as depicted in Fig. 1(a). The domain is periodic in the streamwise (x) and spanwise (z) directions and confined in the depthwise direction (y) by two horizontal walls formed by particles with diameter d positioned on a planar-square lattice with a unit cell length of $1.2d$ and two-dimensional packing density of 0.545. The horizontal position of each wall-particle is randomized within its unit cell. A constant downward force on the top wall, which is otherwise free to move vertically and in the spanwise direction, sets the bed overburden pressure, P_0, which is increased with increasing $\dot{\gamma}$ to maintain a constant volume fraction $\phi \approx 0.58$ of bed particles as shown in Fig. 1(b) and discussed in further detail below. The bottom wall is stationary while the top wall is translated in the streamwise direction with velocity $U = \dot{\gamma}h(t)$, where the time-dependent bed height, $h(t)$, accommodates dilation due to shear and varies in time by $\sim \pm 0.1\%$. The flow domain is $20d$ long, $10d$ wide and $60d$ deep, comprising approximately 12 500 large particles (gray region) for most of the simulations. Bed particles have a uniform diameter-dispersity of $\pm 10\%$ to minimize layering [36]. To ensure homogeneous shear in the presence of gravity, a small streamwise stabilizing force $-k(\dot{\gamma}y_i - u_i)$, where u_i and y_i are the streamwise velocity and height of bed particle i, respectively, and $k = 0.1\,\mathrm{kg/s}$, is applied to each bed particle (but not the percolating fine particles) at each simulation time step [35, 37–39]. This approach produces the desired homogeneous shear flow without altering the flow rheology [40] or segregation [41].

After the sheared bed of large particles reaches steady state, fine particles with identical diameter d_f are randomly positioned just above ($1.02 < y/h < 1.03$) the porous top wall of the bed. All fine particles are given an initial streamwise velocity matching the streamwise velocity of the moving top-wall, which allows them to quickly fall beneath the wall when they are simultaneously released. In order to examine the zero-concentration limit and, thereby, avoid the complications associated with fine particle jamming, fine particles interact with bed particles but not with each other. The number of fine particles depends on R and varies from $\sim 10^3$ ($R = 2$) to $\sim 10^4$ ($R = 10$), which keeps the fine particle volume concentration below 1%. This low concentration prevents the multiple fine particles percolating simultaneously through the bed from significantly altering the flow kinematics and rheology of the bed particles and allows the dynamics of multiple independent fine particles to be computed in one simulation, which is computationally efficient and provides sufficient data for accurate statistics. Doubling the number of fine particles in additional simulations, covering $3 \le R \le 7$ and $1\ \mathrm{s}^{-1} \le \dot{\gamma} \le 40\ \mathrm{s}^{-1}$, does not alter the flow kinematics, the bed rheology, or the measured value of v_p. Simulation times vary with R and $\dot{\gamma}$, and are typically on the order

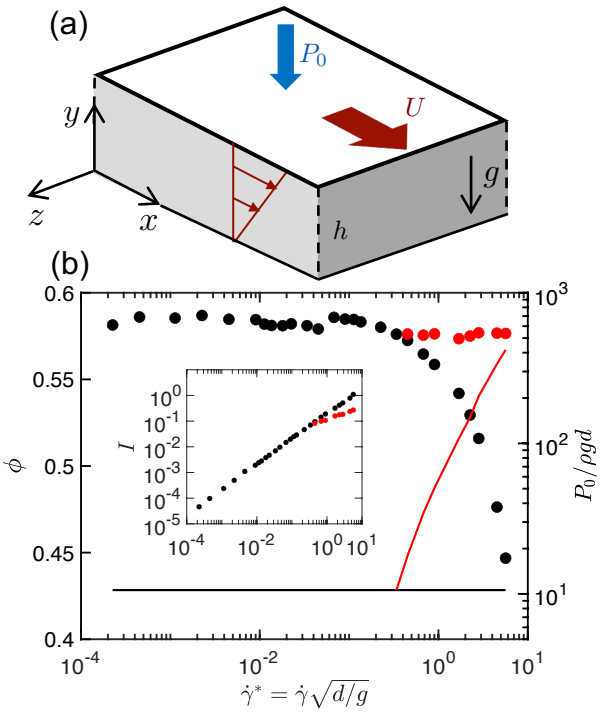

FIG. 1. Simulation conditions. (a) Single fine particles (not shown) percolate under gravity in a confined granular shear flow with a controlled spatially uniform shear rate $\dot{\gamma}$ (see text). (b) Bed particle packing density, ϕ, vs. non-dimensional shear rate $\dot{\gamma}^* = \dot{\gamma}\sqrt{d/g}$ for overburden pressure, P_0, held constant at 1.2 kPa (black line and circles) or gradually increased above 1.2 kPa for $\dot{\gamma}^* > 0.3$ to maintain nearly constant ϕ (red curve and circles). (inset) Inertial number, $I = \dot{\gamma}d/\sqrt{P/\rho}$ vs. $\dot{\gamma}^*$ for constant (black) and increasing (red) P_0.

of 10 s to ensure that most fine particles reach the lower wall. Simulation times for smaller R at lower $\dot{\gamma}^*$ are increased so that the fraction of fine particles re-mobilized by shear induced rearrangement is sufficient for accurate measurement of v_p. For example, the simulation time is increased up to 100 s for $R < 6$ and $\dot{\gamma}^* < 10^{-3}$. Fine-particle motion is characterized by the mean vertical velocity, $v_p = \langle v_i \rangle$, or *percolation* velocity, and the RMS velocity, $v_{\mathrm{rms}} = \langle \sqrt{(v_p - v_i)^2} \rangle$, where v_i is the vertical velocity of fine particle i and brackets indicate ensemble and temporal averaging.

The majority of simulations presented in the paper use the following parameters: bed particle average diameter $d = 5\,\mathrm{mm}$ with 10% uniform polydispersity, acceleration due to gravity $g = 9.81\,\mathrm{m\,s^{-2}}$, restitution coefficient $e = 0.8$, friction coefficient $\mu = 0.5$, and densities of bed (ρ) and fine particle (ρ_f) are both $2\,500\,\mathrm{kg\,m^{-3}}$. Additionally, d, g, e and ρ_f are varied in other simulations to explore their effects on the percolation velocity. The simulations use the Hertz contact model with a Young's modulus of 5×10^7 Pa, and a Poisson's ratio of 0.4. The simulation time step is 5×10^{-6} s to ensure numerical

stability even for the largest size ratios and highest shear rates that are examined.

Previous studies indicate that decreasing ϕ increases v_p in both static [24] and flowing systems [42]. Increasing $\dot{\gamma}^* \equiv \dot{\gamma}\sqrt{d/g}$ with constant $P_0 = 1200\,\mathrm{Pa} \sim 10\rho g d$ [horizontal black line in Fig. 1(b)] increases bed dilation which decreases ϕ [black circles in Fig. 1(b)] for $\dot{\gamma}^* > 0.3$, while the inertial number of the bed particles, $I = \dot{\gamma}d/\sqrt{P/\rho}$, increases linearly [inset of Fig. 1(b)]. In the expression for I, P is the normal stress of bed particles averaged over a $40d$-thick layer in the middle of the bed. For $\dot{\gamma}^* \gtrsim 1$, I tends towards dilute collisional flow [43]. To minimize changes in the pore size distribution due to shear-driven variation in ϕ [24] and to keep the maximum ϕ value closer to that for dense flow, P_0 is increased by a factor of 40 with increasing $\dot{\gamma}^*$ over the range $0.3 < \dot{\gamma}^* < 4$ as indicated in the figure. This procedure keeps ϕ in the range $0.57 < \phi < 0.58$ [red curve and red circles in Fig. 1(b)] and the inertial number in the dense flow range, $\sim 10^{-4} < I <\sim 0.3$.

Vertical velocity—Figure 2 plots the scaled fine-particle vertical velocity, $v_p^* = -v_p/\sqrt{gd}$, versus scaled shear rate, $\dot{\gamma}^* = \dot{\gamma}\sqrt{d/g}$, for $2 \le R \le 10$. As in static beds, fines always percolate downward on average even at the largest $\dot{\gamma}^*$, and v_p^* increases monotonically with increasing R for all $\dot{\gamma}^*$. However, the $\dot{\gamma}^*$-dependence of v_p^* is strongly R-dependent. First, for size ratios in the static-bed passing regime ($R > 6.5 > R_{t0}$ here due to overburden-pressure-driven deformation and polydispersity of bed particles that decreases the minimum pore throat diameter relative to rigid monodisperse bed particles [23]), v_p^* initially remains constant at its static-bed value as $\dot{\gamma}^*$ is increased from zero. Hence, $v_p \propto \sqrt{gd}$ for $R \gtrsim R_t$. However, above $\dot{\gamma}^* \gtrsim 0.03$, v_p^* decreases with increasing $\dot{\gamma}^*$. Second, for size ratios in the static-bed trapping regime ($R \le 6.5$), v_p^* increases from zero with increasing $\dot{\gamma}^*$, similar to segregation with $R \lesssim 2$ [8–10, 12]. However, v_p^* reaches a maximum near $\dot{\gamma}^* \sim 0.1$ and then decreases toward zero with further increase in $\dot{\gamma}^*$. Note that a previously observed $\dot{\gamma}$-independence of v_p for $R \approx 2.5$ [32] results from that study's limited shear rate range, $0.04 < \dot{\gamma}^* < 0.14$, which serendipitously brackets the peak in v_p about which v_p is nearly constant (e.g., see $R = 2$ data in Fig. 2). To test the nondimensionalization of v_p and $\dot{\gamma}$, Fig. 2 also includes data where d and g differ from the values used in the other simulations. This additional data (magenta symbols) overlays the data for $d = 5\,\mathrm{mm}$ and $g = 9.81\,\mathrm{m/s^2}$ at the corresponding R values, indicating that the scaling of v_p and $\dot{\gamma}$ is correct in both low and high $\dot{\gamma}$ regimes.

The value of $\dot{\gamma}^*$ where v_p^* begins to drop decreases with increasing R (dashed curve), e.g., $\dot{\gamma}^* \approx 0.14$ for $R = 2$, while $\dot{\gamma}^* \approx 0.03$ for $R = 6.5$. This sensitivity to R along with the decrease in v_p with increasing $\dot{\gamma}$ for $\dot{\gamma}^* \gtrsim 0.1$ is due to increasing fine-particle velocity fluctuations (characterized by v_{rms}), which frustrate percolation and increase with increasing R or $\dot{\gamma}^*$, as described later. In static beds, a similar decrease in v_p is observed with increasing e for both $4 \le R \le R_t$ [24] and $R > R_t$ [16, 18, 20, 24].

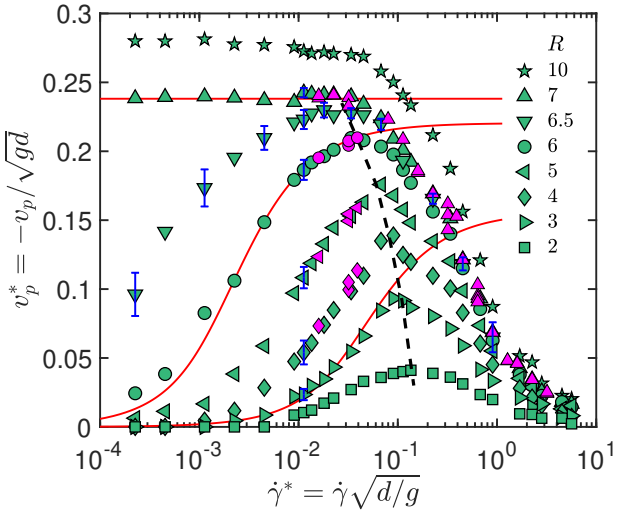

FIG. 2. Scaled fine-particle vertical velocity, $v_p^* = -v_p/\sqrt{gd}$, vs. scaled shear rate, $\dot{\gamma}^* = \dot{\gamma}\sqrt{d/g}$, for various particle size ratios, R, gravitational accelerations, g, and bed particle diameters, d, with restitution coefficient $e = 0.8$. Volume fraction of large particles is kept nearly constant ($0.57 < \phi < 0.58$) by increasing the overburden pressure, P_0, as $\dot{\gamma}$ is increased. Magenta symbols indicate data for $d \in \{2.5, 10, 15\}$ mm and $g \in \{4.91, 19.62, 29.43\}\,\mathrm{m/s^2}$ at $\dot{\gamma} = 1\,\mathrm{s^{-1}}$ for $R \le 6$ and for $1 \le \dot{\gamma} \le 100\,\mathrm{s^{-1}}$ for $R = 7$ that validate the scaling. Dashed black curve approximates maximum v_p^* location for different R. Error bars for selected cases indicate standard error of v_p. Red curves are predictions of the low-shear-rate regime model (Eq. 2) for $R = 3$, 6, and 7.

Figure 2 and previous work in static beds [24] suggest that fine-particle percolation in sheared beds depends on three mechanisms: geometric trapping, which is possible when $R < R_t$; bed particle rearrangement due to shear; and fine-particle velocity fluctuations, which frustrate percolation. The basics are as follows. First, fines with $R < R_t$ that are trapped re-mobilize due to shear-driven bed rearrangements at a rate that is proportional to $\dot{\gamma}$ and increases with R, since passable voids are generated at a higher rate for smaller fines. Second, the average time to pass a passable-void increases with increasing excitation of the fines, i.e., v_{rms}. Consequently, at high shear rates, where trapping times are short for $R < R_t$ and v_{rms} is large ($v_{\mathrm{rms}} \propto \dot{\gamma}$) for all R, v_p decreases with increasing $\dot{\gamma}$.

Low-shear-rate regime—To better understand the dominant physics and develop a model for v_p in this regime, we start with the percolation depth model for $R < R_t$ in static beds, $p(\Delta y) \propto P_p^{\frac{\Delta y}{d}}$, where $p(\Delta y)$ is the probability that a fine particle falls a distance Δy or more

from its starting height without becoming trapped, and P_p represents the probability of a fine passing through a randomly selected pore throat, which is equivalent to the fraction of constrictions with diameters larger than d_f [24]. In static beds, $p(\Delta y)$ is the proportion of fine-particle trajectories that exceed a depth $\geq \Delta y$, assuming that the passage of fines through consecutive pore throats is independent [24, 44]. Since untrapped fines percolate with mean velocity $v_{p,s} = -c_1\sqrt{gd}$ [24], $p(\Delta y)$ can be reformulated as a function of time using $\Delta y = -v_{p,s}t$ as $p(t) \propto P_p^{\frac{-v_{p,s}t}{d}}$, where $p(t)$ is the probability that a fine particle is untrapped after time t. The average vertical velocity over t is then

$$v_p = \frac{v_{p,s}}{t}\int_0^t p(t')\,dt' \propto \frac{d}{t\ln P_p}\left(1 - P_p^{\frac{-v_{p,s}t}{d}}\right). \quad (1)$$

For sheared systems, we assume that the time interval between significant bed rearrangements scales as $t_b = c_2(R)\dot{\gamma}^{-1}$. Substituting t_b for t in Eq. 1 gives v_p as a function of shear rate, bed structure (via P_p) and its variation (via c_2), bed particle diameter, and gravitational acceleration:

$$v_p = \frac{d\dot{\gamma}}{c_2 \ln P_p}\left(1 - P_p^{c_1 c_2\sqrt{\frac{g}{\dot{\gamma}^2 d}}}\right). \quad (2)$$

This relation is alternatively expressed as

$$v_p' = \frac{v_p}{v_{p,s}} = \dot{\gamma}'\left[1 - \exp\left(-1/\dot{\gamma}'\right)\right], \quad (3)$$

where $\dot{\gamma}' = -C\dot{\gamma}\sqrt{d/g}$ with $C^{-1} = c_1 c_2 \ln P_p$ as the single model parameter. Eq. 2 exhibits the appropriate limiting behaviors under its assumption that $v_{\rm rms}$ is small: i) as $\dot{\gamma} \to \infty$ ($t_b \to 0$), $v_p \to v_{p,s} \propto \sqrt{gd}$ for all R; ii) as $\dot{\gamma} \to 0$, $v_p \propto d\dot{\gamma}$ for the trapping regime ($R < R_t$) as in most shear-driven percolation models for small R [8–10, 12] and is independent of g; iii) in the passing regime ($R > R_t$, $P_p = 1$) $v_p \propto \sqrt{gd}$ independent of $\dot{\gamma}$ as in i).

To compare Eq. 2 to our data, we determine P_p by characterizing the pore throat size distribution using Delaunay triangulation [24, 45, 46]. For $\phi \approx 0.58$, P_p is nearly independent of shear rate for $\dot{\gamma}^* \lesssim 0.1$, and increases from 0.17 to 0.93 as R is increased from 2 to 6. From [24], $c_1 = 0.09\sqrt{R}$ for $\phi \approx 0.58$ and $e = 0.8$. Fits of Eq. 2 to simulation results for three R values obtained by adjusting the one free parameter, c_2, match the simulation data at low $\dot{\gamma}^*$, as shown in Fig. 2 (solid curves). The inset in Fig. 3 indicates that P_p increases with R and c_2 decreases with R, as expected.

All data in Fig. 2 is compared to the universal form of the model (Eq. 3) in Fig. 3, which plots the vertical velocity scaled by the untrapped vertical velocity from the static bed, $v_p' = v_p/v_{p,s}$, versus the rescaled shear rate $\dot{\gamma}' = -C\dot{\gamma}^*$. Data for all R as well as varying g and d (magenta) collapse onto the model prediction (red curve) in the low-shear-rate region. For free-sifting cases ($R > 6.5$), $\dot{\gamma}' = \infty$ since $P_p = 1$, and the corresponding symbols fall on the far right of Fig. 3 and approach $v_p' = 1$ (yellow star) in the low-shear-rate regime.

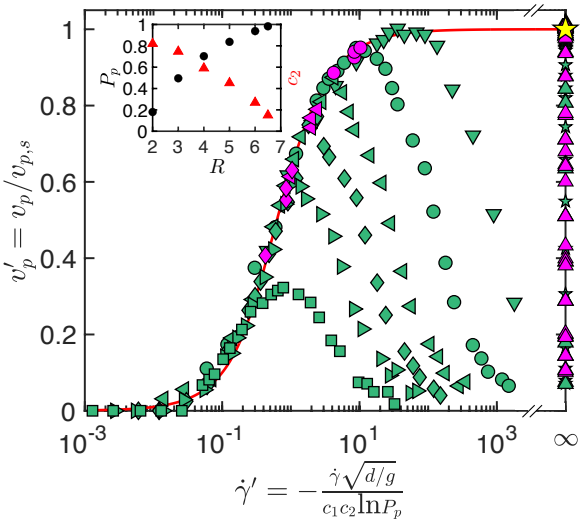

FIG. 3. Fine-particle vertical velocity scaled by vertical velocity of untrapped fines in static bed, $v_p/v_{p,s}$, vs. rescaled shear rate, $\dot{\gamma}'$, showing collapse of all data (symbols) from Fig. 2 in the low-shear-rate-regime onto the prediction of Eq. 3 (red curve). Data include varying R (symbols), and g and d (magenta) for $\phi \approx 0.58$ and $e = 0.8$. Passing regime data ($R > 6.5$) fall on the right boundary since $\dot{\gamma}' = \infty$. Inset: P_p (left: black circle) and c_2 (right: red triangle) vs. R.

High-shear-rate regime—When v_p^* for $\dot{\gamma}^* \gtrsim 0.1$ is plotted versus $\dot{\gamma}^*$ on a log-scale in Fig. 4(a), it is clear that $v_p^* \propto 1/\dot{\gamma}^*$ for $\dot{\gamma}^* \gtrsim 0.4$ and various R, g and d. This behavior is related to increasing fine-particle velocity fluctuations, which frustrate percolation. To demonstrate the relation between $\dot{\gamma}^*$ and $v_{\rm rms}$, Fig. 4(b) plots the scaled vertical root-mean-square velocity fluctuations of fines, $v_{\rm rms}^* = v_{\rm rms}/\sqrt{gd}$, versus $\dot{\gamma}^*$ for various R. For context, $v_{\rm rms}^*$ for *bed* particles (×) increase linearly with $\dot{\gamma}^*$, as would be expected from the corresponding increase in inter-particle collisions. Similarly, for $\dot{\gamma}^* \gtrsim 0.4$, $v_{\rm rms}^* \propto \dot{\gamma}^*$ for all R, indicating that fine-particle velocity fluctuations are driven by the bed-particle velocity fluctuations in the high $\dot{\gamma}^*$ regime. In comparison, for $\dot{\gamma}^* \lesssim 0.1$, gravity-driven fluctuations dominate, so that $v_{\rm rms}^*$ is either constant (free-sifting, $R > 6.5$) or decreases slower than $\dot{\gamma}^*$ (trapping, $R \leq 6.5$) because $v_{\rm rms}^*$ is an average over trapped (smaller bed-driven fluctuations) and untrapped (larger gravity-driven fluctuations) states. Simulations with different g and d values at $R = 7$ [magenta triangles in Fig. 4(b)] confirm the scaling of $v_{\rm rms}$ with $\dot{\gamma}$ and indicate that $v_{\rm rms}$ is g-independent where $v_{\rm rms}^* \propto \dot{\gamma}^*$ but proportional to $\sqrt{gd}$ where $v_{\rm rms}^*$ is constant.

For all $\dot{\gamma}^*$, $v_{\rm rms}^*$ is larger for larger R and approaches a limiting curve for large R, as Fig. 4(b) shows. Addi-

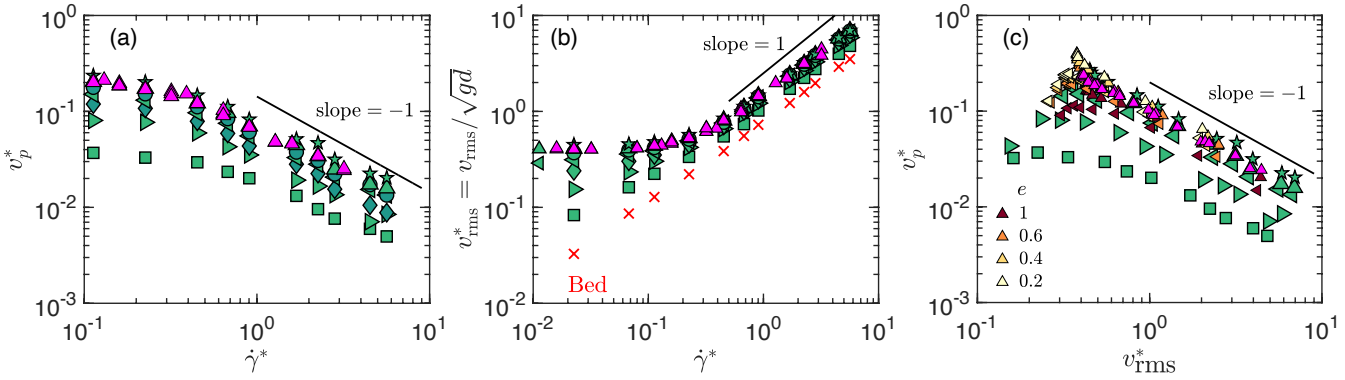

FIG. 4. (a) Scaled fine-particle vertical velocity, $v_p^* = -v_p/\sqrt{gd}$, varies inversely with scaled shear rate, $\dot{\gamma}^* = \dot{\gamma}\sqrt{d/g}$. (b) Scaled fine-particle RMS velocity fluctuations, $v_{\rm rms}^* = v_{\rm rms}/\sqrt{gd}$, increase linearly with $\dot{\gamma}^*$ for $\dot{\gamma}^* \gtrsim 0.4$. Bed particle data (×) shown for comparison. (c) v_p^* varies inversely with $v_{\rm rms}^*$ for various shear rates, and restitution coefficients, e (colors as indicated). Data in (a-c) includes various size ratios $2 \le R \le 10$ (symbols), and g and d values (magenta) as in Fig. 2.

tional simulations with fine-particle density varied by two orders of magnitude ($250\,\mathrm{kg\,m^{-3}}$ to $2.5 \times 10^4\,\mathrm{kg\,m^{-3}}$) at constant R change $v_{\rm rms}$ by $< 7\%$ (v_p is also minimally affected), indicating that the increase in $v_{\rm rms}$ with increased R is due to decreased fine-particle diameter (i.e., smaller fines are less constrained by bed particles than larger fines) rather than decreased fine-particle mass.

Having demonstrated the linear dependence of $v_{\rm rms}$ on shear rate at high $\dot{\gamma}$, Fig. 4(c) tests our hypothesis that the mean vertical velocity decreases with increasing $v_{\rm rms}$. Indeed, the data show that $v_p^* \propto 1/v_{\rm rms}^*$ when $v_{\rm rms}^* \gtrsim 0.4$ for all R. In dimensional form, $v_p \propto gd/v_{\rm rms} \propto g/\dot{\gamma}$, where the linear dependence of v_p versus $\dot{\gamma}$ on g alone at high $\dot{\gamma}$ contrasts with the low-shear-rate scaling of v_p with $\sqrt{gd}$ in the free-sifting regime and with d alone in the trapping regime. Equally significant, Fig. 4(c) also includes data for varying restitution coefficient between bed and fine particles, $0.2 \le e \le 1$, for $R = 5$ and 7. Low restitution reduces $v_{\rm rms}$ for large $\dot{\gamma}$ such that different combinations of e and $\dot{\gamma}$ producing the same $v_{\rm rms}$ yield the same v_p. Hence, $v_{\rm rms}$ determines v_p in the high shear-rate regime ($\dot{\gamma}^* \gtrsim 0.4$).

Discussion—This study of gravity-driven percolation of single non-cohesive fine particles in sheared granular beds reveals different dominant physics at low and high shear rates. For low shear rates, $\dot{\gamma}\sqrt{d/g} \lesssim 0.1$, as $\dot{\gamma}$ increases from zero, bed-particle rearrangements due to shear reduce fine-particle trapping to increase the mean vertical velocity, v_p. A statistical model of this mechanism (Eqs. 2 or 3) accurately predicts v_p for a wide range of conditions. In the high-shear-rate regime, $\dot{\gamma}\sqrt{d/g} \gtrsim 0.1$, increasing $\dot{\gamma}$ results in increasing fine-particle velocity fluctuations which frustrate percolation such that $v_p \propto 1/v_{\rm rms} \propto 1/\dot{\gamma}$ (Fig. 4).

Beyond its relevance to macroscale percolation, gravitational-field-driven transport of fines in sheared large-particle beds shares intriguing similarities with electric-field-driven conduction in solids, where conductivity is the product of mobility and carrier concentration, see, e.g., [47]. For $R > R_t$, the granular system is metal-like in that fine-particles are never trapped and their mobility decreases with increasing $v_{\rm rms}$ [Fig. 4(c)]. The $v_p^* \propto 1/v_{\rm rms}^*$ dependence for fine-particle mobility is analogous to lattice scattering in the Drude model [48] for electron transport due to an electric field, E. In the model, the mean electron momentum is $p = m_e v = qE\tau$, where m_e and q are the electron mass and charge, respectively, and τ is the time between collisions with lattice particles. Replacing v with v_p, qE/m_e with g, and τ with $d/v_{\rm rms}$ (since the fine-particle mean free path is proportional to d) yields the observed scaling $v_p \propto gd/v_{\rm rms}$ for fines. The near constant v_p^* region evident in Fig. 2 for $R \in \{7, 10\}$ and $\dot{\gamma}^* \lesssim 0.1$ occurs because $v_{\rm rms} \neq 0$, even at $\dot{\gamma}^* = 0$ in static beds, due to $\mathcal{O}(\sqrt{gd})$ velocity fluctuations during free sifting. It is only when $\dot{\gamma}^* > 0.1$ that shear-induced fluctuations of $\mathcal{O}(d\dot{\gamma})$ become significant enough relative to $\sqrt{gd}$ that v_p decreases.

For $R < R_t$, the granular system is semiconductor-like in that the fraction of time fine-particles are untrapped increases with $\dot{\gamma}$, analogous to the increase in electron-concentration in the conduction band of an n-type semiconductor with increasing temperature due to ionization. For sufficiently large $\dot{\gamma}^*$, fines are effectively never trapped, resembling the saturation region in doped semiconductors where carrier concentration is constant, and $v_p \propto 1/v_{\rm rms}$ as for the metal-like $R > R_t$ case due to enhanced scattering. The $R = 6.5$ case is notable in that with increasing $\dot{\gamma}^*$, "saturation" occurs before $v_{\rm rms}$ begins to increase [see above and Fig. 4(b)] and mobility to decrease, resulting in a plateau in v_p for $0.01 < \dot{\gamma}^* < 0.05$.

This work only begins to explore the intriguing physics of fine-particle percolation in driven granular systems, and many questions and challenges remain. For instance, our model and scalings accurately capture the dependence of v_p on $\dot{\gamma}$, d, and g, but understanding how to incorporate e and R as well as cohesion in expres-

sions for v_p^* and v_{rms} is likely to be non-trivial, although analogies with conduction in solids may be fruitful, as outlined above. Additionally, extending our single-fine-particle-limit results to finite fine-particle concentrations, c_f, would also be valuable and potentially analogous to strongly correlated electron systems. Preliminary heap flow simulations with $R > 4$ and global c_f up to 30% exhibit high-shear regions with local $c_f < 5\%$ where insights from the single-fine-particle limit are likely applicable, but also low-shear regions, where fines pack densely around large particles, forming a continuous fine-particle phase that greatly reduces their vertical mobility.

We thank John P. Hecht, Alexander M. Fry, Jörg Theuerkauf, and Yi Fan for insightful discussions. This material is based upon work supported by the National Science Foundation under Grant No. CBET-2203703.

* umbanhowar@northwestern.edu

[1] R. M. Iverson, The physics of debris flows, Rev. Geophys. **35**, 245 (1997).
[2] P. Frey and M. Church, How river beds move, Science **325**, 1509 (2009).
[3] C. Johnson, B. Kokelaar, R. M. Iverson, M. Logan, R. LaHusen, and J. Gray, Grain-size segregation and levee formation in geophysical mass flows, J. Geophys. Res. Earth Surf. **117** (2012).
[4] J. Ottino and D. Khakhar, Mixing and segregation of granular materials, Annu. Rev. Fluid Mech. **32**, 55 (2000).
[5] J. M. Ottino and R. M. Lueptow, On mixing and demixing, Science **319**, 912 (2008).
[6] J. M. N. T. Gray, Particle segregation in dense granular flows, Annu. Rev. Fluid Mech. **50**, 407 (2018).
[7] P. B. Umbanhowar, R. M. Lueptow, and J. M. Ottino, Modeling segregation in granular flows, Annu. Rev. Chem. Biomol. Eng. **10**, 129 (2019).
[8] B. Marks, P. Rognon, and I. Einav, Grainsize dynamics of polydisperse granular segregation down inclined planes, J. Fluid Mech. **690**, 499 (2012).
[9] Y. Fan, C. P. Schlick, P. B. Umbanhowar, J. M. Ottino, and R. M. Lueptow, Modelling size segregation of granular materials: the roles of segregation, advection and diffusion, J. Fluid Mech. **741**, 252 (2014).
[10] D. R. Tunuguntla, O. Bokhove, and A. R. Thornton, A mixture theory for size and density segregation in shallow granular free-surface flows, J. Fluid Mech. **749**, 99 (2014).
[11] A. M. Scott and J. Bridgwater, Interparticle percolation: a fundamental solids mixing mechanism, Ind. Eng. Chem. Fundam. **14**, 22 (1975).
[12] T. Trewhela, C. Ancey, and J. Gray, An experimental scaling law for particle-size segregation in dense granular flows, J. Fluid Mech. **916**, A55 (2021).
[13] C. P. Schlick, Y. Fan, A. B. Isner, P. B. Umbanhowar, J. M. Ottino, and R. M. Lueptow, Modeling segregation of bidisperse granular materials using physical control parameters in the quasi-2d bounded heap, AIChE J. **61**, 1524 (2015).
[14] J. Bridgwater and N. Ingram, Rate of spontaneous interparticle percolation, Trans. Inst. Chem. Eng. **49**, 163 (1971).
[15] D. Wilkinson and S. F. Edwards, Spontaneous interparticle percolation, Proc. Math. Phys. Eng. Sci. **381**, 33 (1982).
[16] F. Lominé and L. Oger, Dispersion of particles by spontaneous interparticle percolation through unconsolidated porous media, Phys. Rev. E **79**, 051307 (2009).
[17] J. Li, A. Yu, J. Bridgwater, and S. L. Rough, Spontaneous inter-particle percolation: A kinematic simulation study, Powder Technol. **203**, 397 (2010).
[18] J. Bridgwater, N. Sharpe, and D. Stocker, Particle mixing by percolation, Trans. Inst. Chem. Eng. **47**, 114 (1969).
[19] C. Ghidaglia, L. de Arcangelis, J. Hinch, and É. Guazzelli, Transition in particle capture in deep bed filtration, Phys. Rev. E **53**, R3028 (1996).
[20] I. Ippolito, L. Samson, S. Bourles, and J.-P. Hulin, Diffusion of a single particle in a 3d random packing of spheres, Eur. Phys. J. E **3**, 227 (2000).
[21] S. Remond, DEM simulation of small particles clogging in the packing of large beads, Phys. A: Stat. Mech. Appl. **389**, 4485 (2010).
[22] J. Dodds, The porosity and contact points in multicomponent random sphere packings calculated by a simple statistical geometric model, J. Colloid Interface Sci. **77**, 317 (1980).
[23] D. R. Vyas, S. Gao, P. B. Umbanhowar, J. M. Ottino, and R. M. Lueptow, Poly-dispersity and deformation effects on pore throat size in granular beds (2024), arXiv:2401.02534 [cond-mat.soft].
[24] S. Gao, J. M. Ottino, P. B. Umbanhowar, and R. M. Lueptow, Percolation of a fine particle in static granular beds, Phys. Rev. E **107**, 014903 (2023).
[25] C. Bemrose and J. Bridgwater, A review of attrition and attrition test methods, Powder Technol. **49**, 97 (1987).
[26] D. Schulze, *Powders and bulk solids: Behaviour, characterization, storage and flow* (Springer, Berlin, 2008).
[27] J. C. Phillips, A. J. Hogg, R. R. Kerswell, and N. H. Thomas, Enhanced mobility of granular mixtures of fine and coarse particles, Earth Planet. Sci. Lett. **246**, 466 (2006).
[28] E. Linares-Guerrero, C. Goujon, and R. Zenit, Increased mobility of bidisperse granular avalanches, J. Fluid Mech. **593**, 475 (2007).
[29] R. Chassagne, P. Frey, R. Maurin, and J. Chauchat, Mobility of bidisperse mixtures during bedload transport, Phys. Rev. Fluids **5**, 114307 (2020).
[30] W. E. Dietrich, J. W. Kirchner, H. Ikeda, and F. Iseya, Sediment supply and the development of the coarse surface layer in gravel-bedded rivers, Nature **340**, 215 (1989).
[31] P. R. Wilcock, Two-fraction model of initial sediment motion in gravel-bed rivers, Science **280**, 410 (1998).
[32] N. Khola and C. Wassgren, Correlations for shear-induced percolation segregation in granular shear flows, Powder Technol. **288**, 441 (2016).
[33] G. I. Tardos, S. McNamara, and I. Talu, Slow and intermediate flow of a frictional bulk powder in the couette geometry, Powder Technol. **131**, 23 (2003).
[34] C. Kloss, C. Goniva, A. Hager, S. Amberger, and S. Pirker, Models, algorithms and validation for open-source dem and cfd–dem, Prog. Comput. Fluid Dyn. **12**, 140 (2012).

[35] A. M. Fry, P. B. Umbanhowar, J. M. Ottino, and R. M. Lueptow, Effect of pressure on segregation in granular shear flows, Phys. Rev. E **97**, 062906 (2018).

[36] L. Staron and J. Phillips, Segregation time-scale in bidisperse granular flows, Phys. Fluids **26**, 033302 (2014).

[37] E. Lerner, G. Düring, and M. Wyart, A unified framework for non-brownian suspension flows and soft amorphous solids, Proc. Natl. Acad. Sci. **109**, 4798 (2012).

[38] A. H. Clark, J. D. Thompson, M. D. Shattuck, N. T. Ouellette, and C. S. O'Hern, Critical scaling near the yielding transition in granular media, Phys. Rev. E **97**, 062901 (2018).

[39] K. Saitoh and B. P. Tighe, Nonlocal effects in inhomogeneous flows of soft athermal disks, Phys. Rev. Lett. **122**, 188001 (2019).

[40] L. Jing, J. M. Ottino, R. M. Lueptow, and P. B. Umbanhowar, Rising and sinking intruders in dense granular flows, Phys. Rev. Res. **2**, 022069 (2020).

[41] L. Jing, J. M. Ottino, R. M. Lueptow, and P. B. Umbanhowar, A unified description of gravity-and kinematics-induced segregation forces in dense granular flows, J. Fluid Mech. **925**, A29 (2021).

[42] K. van der Vaart, P. Gajjar, G. Epely-Chauvin, N. Andreini, J. Gray, and C. Ancey, Underlying asymmetry within particle size segregation, Phys. Rev. Lett. **114**, 238001 (2015).

[43] Y. Forterre and O. Pouliquen, Flows of dense granular media, Annu. Rev. Fluid Mech. **40**, 1 (2008).

[44] P. Meakin and R. Jullien, Simulation of small particle penetration in a random medium, J. Phys. France **51**, 2673 (1990).

[45] R. Al-Raoush, K. Thompson, and C. S. Willson, Comparison of network generation techniques for unconsolidated porous media, Soil. Sci. Soc. Am. J. **67**, 1687 (2003).

[46] N. Reboul, E. Vincens, and B. Cambou, A statistical analysis of void size distribution in a simulated narrowly graded packing of spheres, Granul. Matter **10**, 457 (2008).

[47] N. W. Ashcroft and N. D. Mermin, *Solid state physics* (Holt, Rinehart and Winston, New York, NY, 1976).

[48] P. Drude, Zur elektronentheorie der metalle, Annalen der Physik **306**, 566 (1900).